KINEMATIC DIFFUSION IN QUASI-STATIC GRANULAR DEFORMATION

by A. K. DIDWANIA

(*Department of Mechanical and Aerospace Engineering, University of California, San Diego, La Jolla, California* 92093-0411, *USA*)

K. LEDNICZKY

(*Department of Mechanics, Technical University of Budapest, Hungary*)

and J. D. GODDARD

(*Department of Mechanical and Aerospace Engineering, University of California, San Diego, La Jolla, California* 92093-0411, *USA*)

[Received 17 February 2000. Revise 30 October 2000]

Summary

A statistical–mechanical model is proposed for the quasi-static deformation of granular assemblies, in which particle motion is decomposed into a mean-field contribution, given by the macroscopically imposed deformation, together with fluctuations representing stochastic multiparticle mechanics. This leads to the notion of kinematic diffusion and the postulate of a convection–diffusion (Fokker–Planck) equation for various configurational probability distributions. Based on statistics obtained from numerical simulation of a frictional-sphere assembly, self diffusivities and pair diffusivities are derived for various homogeneous deformations, including 'cubical-triaxial' strains as well as simple shear. Among the important findings are (i) diffusive motions are found generally to be small relative to convection, suggesting that the mean-field approximation should be quite accurate, and (ii) pair correlations are weak, implying that two-particle and higher-order cluster diffusivities follow from single-particle diffusivities. Based on the idea of negligible diffusion, a semi-theoretical model of granular plasticity with fabric evolution is proposed, as an extension of the exact mean-field model of Jenkins and Strack. It is concluded, however, that even weak diffusion effects might have important consequences for certain continuum properties, because of the influence on unstable equilibrium configurations. This is supported by comparison of various mean-field kinematic estimates of Reynolds dilatancy to a more accurate estimate obtained from the mechanics simulation for a dense random packing of spheres.

1. Introduction

The 'mean-field approximation' (MFA) has found widespread applicability in the estimation of effective-continuum properties of granular assemblies such as elasticity, plastic yield and scalar conductivity (**1** to **5**). The basic idea underlying the approximation is that local gradients, represented by differences between adjacent particles in a granular assembly, are given directly by global or mean gradients, for quantities such as temperature, electrical potential or mechanical

displacement. In general, the MFA does not satisfy local balance (Kirchhoff's laws, Newton's laws, etc.) at the single-particle level and, hence, will fail in circumstances where departures from the mean, as represented by 'fluctuations', become important (**6**). We recall that the analytic MFA (**4**) for the small-strain elastoplasticity of frictional–elastic sphere assemblies, particularly relevant to the present work, is restricted to the (Hertz–Mindlin) regime where both volume and shear strains are of order $(p/E)^{2/3} \ll 1$, p denoting isotropic confining pressure and E a representative Young's modulus of the particles. On the other hand, our previous numerical simulations (**5**, **7**) as well as those to be discussed below, also restricted to the regime $(p/E) \ll 1$, are applicable to much larger plastic shear strains and include comparable volume strains arising from Reynolds dilatancy. Thus, the theory of Jenkins and Strack (**4**) represents a small-strain asymptote for our numerical simulations. In that regard, we note that their stress ratios (q/p in (**4**, Fig. 6)) achieve values of order unity at large plastic strains, which are comparable to those of Goddard and Didwania (τ'/p in (**7**, Figs 5 and 6), where $\tau' = |\mathbf{T}'| = 2\sqrt{\frac{2}{3}}\, q$). In the following, we focus on the the rigid-particle limit $p/E \to 0$, where the MFA assigns to the ith particle, with centroid at position $\mathbf{x}_i$, $i = 1, 2, \ldots$ in a homogeneously deforming assembly, the linear and angular velocities

$$\overline{\mathbf{u}}_i = \overline{\mathbf{u}}(\mathbf{x}_i), \quad \text{where} \quad \overline{\mathbf{u}}(\mathbf{x}) = \mathbf{L}\mathbf{x}, \quad \text{and} \quad \mathbf{w}_i \equiv \mathbf{w} := \text{vec}\{\mathbf{W}\}$$

derived, respectively, from the global velocity gradient and vorticity,[†]

$$\mathbf{L} := (\nabla \overline{\mathbf{u}})^T \quad \text{and} \quad \mathbf{W} := \tfrac{1}{2}(\mathbf{L} - \mathbf{L}^T), \tag{1}$$

where the global gradient is assumed to satisfy the dilatancy constraint. In general, the exact particle velocities are given instead by

$$\mathbf{u}_i = \overline{\mathbf{u}}_i + \mathbf{u}_i' \quad \text{and} \quad \mathbf{w}_i = \mathbf{w} + \mathbf{w}_i', \tag{2}$$

where primes denote fluctuations necessary to satisfy local equilibrium, that is, balance of linear and angular momentum on particle $i = 1, 2, \ldots$. Such fluctuations are in fact the object of most kinetic theories or numerical simulations of molecular or particulate systems. In particular, the quasi-static algorithm employed in (**5**, **7**) determines the fluctuations necessary to achieve static equilibrium following each incremental strain ($\mathbf{L}\Delta t$) imposed in time step Δt of a given deformation history. In the present work, we employ the same technique to obtain various autocorrelations of the fluctuations and, hence, an associated set of translational diffusivities. Similar ideas apply to the various configurational degrees of freedom defining arbitrary clusters of particles, and we discuss below the computations of 'pair' diffusivities for nearest neighbours. Also, we consider certain statistics of the associated Delaunay tetrahedra, which we recall were employed in the mean-field estimate of (**6**) for the dilatancy of sphere assemblies. As will be seen below, the mean-field estimate can be improved by making use of more accurate statistics for random packings, but the significant differences between our improved estimate and more complete mechanics simulations suggest that fluctuations, although nominally small, may have important effects on the micromechanics.

2. Statistical mechanics

Let $\mathbf{q}$ denote a set of coordinates defining an arbitrary subset of N particles in a particle assembly, for example, the set of centres and (Euler) orientation angles, $\mathbf{q} = \{\mathbf{x}_i, \alpha_i, \beta_i, \gamma_i : i = 1, \ldots, N\}$. Then

[†] vec{**W**} denotes the 'axial' vector of **W**, such that $\mathbf{W}\mathbf{a} = \mathbf{w} \wedge \mathbf{a}$ for all vectors **a**.

the quasi-static configurational evolution (that is, the 'dynamics') of a statistically homogeneous assembly of rigid frictional particles must be given by a set of differential equations of the general form

$$\overset{\circ}{\mathbf{q}} = \mathbf{v}(\mathbf{q}; \mathbf{S}), \tag{3}$$

where $\overset{\circ}{\mathbf{q}}$ denotes time rate of change relative to a reference frame in which $\mathbf{W} \equiv \mathbf{0}$ (the Jaumann rate), and $\mathbf{S} = \frac{1}{2}(\mathbf{L} + \mathbf{L}^T) \equiv \mathbf{L}$ is velocity gradient, hence, deformation rate relative to the same frame. The set (3), which incorporates the rotational invariance required by frame indifference (**8**), is to be contrasted to the evolution equation in the full phase space (of coordinates and momenta) for systems where inertia is important. Apart from the difference in the order of the differential equations involved and the frame indifference, (3) are also subject to quasi-static scaling common to several particulate systems, for example, the 'Stokesian dynamics' of suspensions (**9**), resulting from the fact that $\mathbf{v}$ must be homogeneous of degree one in $\mathbf{S}$. Hence, time t can be replaced by a (plastic) strain

$$\gamma = \int_0^t |\mathbf{S}^\diamond| \, dt \tag{4}$$

(denoted by γ' in (**7**)) and $\mathbf{S}$ by the strain-like tensor $\mathbf{E} \equiv \mathbf{S}/|\mathbf{S}^\diamond|$, where, as below, we denote the deviator of second-rank tensors $\mathbf{A}$ by

$$\mathbf{A}^\diamond := \mathrm{dev}\{\mathbf{A}\} \equiv \mathbf{A} - \tfrac{1}{3}\mathrm{tr}\{\mathbf{A}\}\mathbf{1}$$

and the modulus (trace norm) by $|\mathbf{A}| = (\mathrm{tr}\{\mathbf{A}^T\mathbf{A}\})^{1/2}$. Also, except when necessary for clarity, we suppress notation for components of vectors and tensors, denoting the tensor product of vectors $\mathbf{u}$ and $\mathbf{v}$ by $\mathbf{u} \otimes \mathbf{v} = (u^\alpha v^\beta)$, where Greek indices represent tensor components (contravariant, in the form just cited.) We recall that the dilatancy of a granular medium (**7**), $d\epsilon_V/d\gamma \equiv \mathrm{tr}\{\mathbf{E}\}$, is determined by $\mathbf{E}^\diamond$, so that dependence on $\mathbf{E}$ in (3) reduces to a dependence on $\mathbf{E}^\diamond$ alone. The obvious generalization of (2) is the Langevin-type equation obtained by setting

$$\mathbf{v}' = \mathbf{v} - \overline{\mathbf{v}} \tag{5}$$

in (3), where $\mathbf{v}$ is given by (3), $\overline{\mathbf{v}}$ is mean-field motion, and $\mathbf{v}'$ is the fluctuation resulting from the multi-body mechanics.

2.1 *A diffusion approximation*

We postulate that the above fluctuations represent a stochastic diffusion in configuration space, with statistical mechanics described by the Fokker–Planck (or Kolmogorov) equation (**10**, **11**)

$$\frac{\partial P}{\partial t} + \nabla_q \cdot \overline{\mathbf{v}} P = \nabla_q \cdot \mathbf{D} \nabla_q P \tag{6}$$

for the probability distribution $P(\mathbf{q}, t)$ of $\mathbf{q} = (q^\alpha)$, where ∇_q and $\mathbf{D} = (D^{\alpha\beta})$ denote the associated configurational gradient and diffusivity tensor, respectively. This form of diffusion, which we designate as *kinematic*, results essentially from the imposition of motion on a spatially disordered

system, distinguishing it from that associated with random thermal motion which persists even in systems at rest. A similar kinematic diffusion arises from multi-body Stokesian hydrodynamics in dense suspensions and exhibits the same scaling with representative particle dimension a and shear rate $\dot{\gamma}$ (**12** to **14**). Whatever their origins, we recall that diffusivities for stationary–random fluctuations (**10**, **11**) follow from integrals of the form

$$\mathbf{I} \equiv \int_0^\infty \mathbf{C}(\tau)\, d\tau \tag{7}$$

of the velocity autocorrelation

$$\mathbf{C}(\tau) = \langle \mathbf{v}'(t)\mathbf{v}'(t+\tau) \rangle \tag{8}$$

where angle brackets $\langle\ \rangle$ denote ensemble averages and we assume the integrals are well defined. With the standard ergodic hypothesis the latter is identified with the time average

$$\mathbf{C}(\tau) = \lim_{T\to\infty} \frac{1}{T} \int_0^T \mathbf{v}'(t) \otimes \mathbf{v}'(t+\tau)\, dt.$$

In the following, we employ an appropriate modification of this formalism to extract various diffusivities from numerical simulations for sphere assemblies. We note that the velocity autocorrelations in (7) provide a valid definition of diffusivity only if mean strains $|\mathbf{S}(t)\delta t|$ occurring in the characteristic decay time δt of $\mathbf{C}(t)$ (**11**, **15**) are small, which, as will be seen below, appears to be the case with our simulations. Under the quasi-static scaling $t \to \gamma$ discussed above, various translational diffusivities can be expressed as $\dot{\gamma} a^2 \mathbf{D}$, where $\dot{\gamma} \equiv |\mathbf{S}^\diamond|$ is the shear rate (**7**) corresponding to (4), a is characteristic particle radius and $\mathbf{D}$ is a non-dimensional tensor. The characteristic values of $\mathbf{D}$, representing inverse 'Péclet' numbers, serve to indicate the importance of diffusive motion relative to mean motion and, as pointed out below, are found in the present study to be remarkably small.

3. Diffusivities from simulations

We employ the quasi-static simulation of Goddard and Didwania (**7**) for idealized nearly rigid spheres, with many more spheres and smaller total strains. The spheres are assigned a miniscule Hookean contact compliance (that is, large stiffness) to avoid static indeterminacy. We adopt the stiffnesses, the constant confining pressure and the non-dimensional scaling of (**7**), so that the representative particle radius equals unity, the normal and tangential stiffnesses are $k_n = 1$ and $k_t = 0{\cdot}8$, respectively, and the non-dimensional isotropic confining pressure based on actual particle radius and normal stiffness is $p = 4 \times 10^{-5}$. The computational cell, one member of a space-filling periodic array, contains 500 equi-sized spheres. The initially cubic cell is subject to the mean deformation of the assembly, with the deviator $\mathbf{E}^\diamond$ specified and the dilatancy computed so as to maintain a constant mean pressure p. Thus, the simulation represents a kinematically controlled deformation, with stress ratios being allowed to vary accordingly. Initially random isotropic assemblies, generated by the packing algorithm of (**7**), were subject to total plastic strains (4) $\gamma = 0{\cdot}02$, in strain increments $\Delta\gamma = 0{\cdot}0002$. The computed quantities reported below represent averages over five different random initial packings for each of the parameter combinations listed in Table 1, which involve some 120 separate runs. Our choice of total plastic strain and the strain

step was dictated by limitations on computer time, a typical run for a single realization requiring approximately 15 minutes of Cray YMP time. In Table 1, the first two columns indicate the applied deviatoric strain

$$\mathbf{E}^{\diamond} = \mathbf{U}\cos\phi + \mathbf{P}\sin\phi, \tag{9}$$

where

$$\mathbf{U} = -\sqrt{2/3}\,\mathrm{diag}\{1, -\tfrac{1}{2}, -\tfrac{1}{2}\} \quad \text{and} \quad \mathbf{P} = -\sqrt{1/2}\,\mathrm{diag}\{0, 1, -1\} \tag{10}$$

with $\mathbf{U}$ and $\mathbf{P}$ representing (axisymmetric) uniaxial compression and planar compression (or extension), respectively, and corresponding to the 'triaxial' and 'pure shear' or 'plane-strain' states of soil mechanics, and

$$\mathbf{B} = -\sqrt{2/3}\ \mathrm{diag}\{\tfrac{1}{2}, \tfrac{1}{2}, -1\} \tag{11}$$

representing an equibiaxial compression equivalent to $-\mathbf{U}$ (**7**). Here ϕ (in degrees) denotes the so-called Lode angle (**7**), given in terms of the third invariant of $\mathbf{E}$ as

$$\phi = \tfrac{1}{3}\cos^{-1}\{3\sqrt{6}\ \det(\mathbf{E})\} \tag{12}$$

while μ and ρ denote (Coulomb) friction coefficient and density (or particulate volume fraction), respectively. The symbol $\mathbf{G}$ in Table 1 represents simple shear having deviatoric velocity gradient

$$\mathbf{L}^{\diamond} = \frac{|\mathbf{S}^{\diamond}|}{\sqrt{2}} \begin{pmatrix} 1 & 0 & 1 \\ 0 & 0 & 0 \\ -1 & 0 & -1 \end{pmatrix}, \tag{13}$$

with symmetric part equivalent to $\mathbf{P}$ in (10), and antisymmetric part that sets $\mathbf{G}$ off from the other deformations (**7**) considered here. As in (**7**), the coordinate axes implied in (9) to (11) and (13) are taken parallel to the edges of an initially cubic computational cell that subsequently deforms according to the applied deformation. We modify and discretize (7) and (8) via relations of the form

$$\overline{\mathbf{C}}_{AB}(\hat{\tau}) = \frac{1}{\hat{T} - \hat{\tau}} \sum_{\hat{t}=0}^{\hat{T}-\hat{\tau}} \mathbf{v}'_i(\hat{t}) \otimes \mathbf{v}'_j(\hat{t} + \hat{\tau}) \quad \text{for} \quad i \in A,\ j \in B \tag{14}$$

and

$$\mathbf{C}_{AB}(\hat{\tau}) = \frac{1}{N_{AB}} \sum_{AB} \overline{\mathbf{C}}_{AB}(\hat{\tau}). \tag{15}$$

Then

$$\mathbf{I}_{AB} = \int_0^{T/2} \mathbf{C}_{AB}(\tau)\, d\tau \tag{16}$$

is evaluated by a simple trapezoid-rule quadrature based on points at $\hat{\tau}$. Carats $\hat{}$ in (14) and (15) denote integer multiples of the basic time step (or strain increment $\Delta\gamma$) corresponding to the discretization of t, τ and T, where T is duration (total shear strain γ) of the deformation. Thus,

Table 1 Parameters of the simulations

$\mathbf{E}^{\diamond}$	(ϕ)	μ	ρ
U	(0)	0	0·56
P	(30)	0·3	0·63
G	(30)	0·5	
B	(60)		

(14) represents a time average over the maximal range $T - \tau$ permissible for t, and the double average implied by (14) and (15) is analogous to that employed in the numerical simulation of molecular fluids (**16**, pp. 196 ff.) to mitigate the effects of small samples. The subscripts $i \in A$ represent a given set of particles A, and $j \in B$ another set B, while N_{AB} denotes the number of such pairs. In the present analysis, we take A to be any particle in the assembly, as represented by the periodic simulation cell, and then choose

1. $B \equiv A$, with $N_{AB} =$ the number of particles in a simulation cell, or
2. $B =$ the set of nearest neighbours of A, as given by Delaunay triangulation (**17**), with $N_{AB} =$ the number of distinct nearest-neighbour pairs in a simulation cell.

We can then identify 'self' diffusivities, corresponding to $\mathbf{q} = \mathbf{x}$, $\mathbf{v} = \mathbf{u}$, P the single-particle distribution function in (6): $\mathbf{D}_{AA} \equiv \mathbf{I}_{AA}$ corresponding to case 1 above, and pair diffusivities for $\mathbf{q} = \mathbf{x}_A - \mathbf{x}_B$, etc., in (6); $\mathbf{D}_{AB} = 2(\mathbf{I}_{AA} - \mathbf{I}_{AB})$, corresponding to case 2 above (**10**, **16**, **18**). As discussed below, our simulations suggest that $|\mathbf{I}_{AB}| \ll |\mathbf{I}_{AA}|$. We have also calculated analogous rotational diffusivities based on the autocorrelations of angular velocities $\mathbf{w}'$, but these are so small as to be relatively uninteresting for the present purposes and will not be reported here.

3.1 *Representative diffusivities*

To assess the possible effects of strain-induced anisotropy, we decompose various diffusivities into the *mean* or 'spherical' part,

$$D_0 = \tfrac{1}{3}\mathrm{tr}\{\mathbf{D}\} = \tfrac{1}{3}(D_{11} + D_{22} + D_{33}),$$

and we further identify

$$D_1 = \tfrac{2}{3}(D_{11}^2 + D_{22}^2 + D_{33}^2 - D_{11}D_{22} - D_{11}D_{33} - D_{22}D_{33})^{1/2} \tag{17}$$

as one contribution to the anisotropy, and

$$D_2 = \{2(D_{12}^2 + D_{13}^2 + D_{23}^2)\}^{1/2} \tag{18}$$

as another. Cartesian components are intended, with axes which lie along the edges of the original undeformed computational cell and which correspond to the principal axes of $\mathbf{S}$ in the case of the

cubical-triaxial deformations **U**, **P** and **B** of Table 1. For those special deformations D_2 provides one measure of non-coaxiality between **D** and **S**, which, given the inherent symmetry, one expects to be negligible. In the following we refer to D_1 as 'anisotropy' and to D_2 as 'non-coaxiality', although the latter is not strictly correct[‡] for the simple shear **G**. We note that, although (17) and (18) are coordinate specific, the quantity

$$D_1^2 + D_2^2 = \tfrac{2}{3}\mathrm{tr}\{\mathbf{D}^{\diamond 2}\} \tag{19}$$

is invariant. Figure 1 shows a representative autocorrelation for one single-particle velocity component *vs.* the delay, expressed as number of strain increments $\hat{T}$. The figure shows a remarkably rapid decay, on a scale comparable to the shortest strain increment, which we take as justification for our use of (7) and, hence, (16). Next, Figs 2 and 3 show the trend of various diffusivities with strain, *vs.* $\hat{T}$, presented at intervals of 10 steps to avoid inessential detail, and the initial point $\hat{T} = 50$ on the abscissa represents the smallest number of points employed for the averages in (14) to (16). The 'anisotropy' D_1, effectively too small to be perceptible in Figs 2 and 3, is not shown. These plots indicate that

1. all diffusivities appear eventually to attain constant values, on (strain) scales that presumably represent large-scale rearrangements necessary to achieve a steady state,
2. diffusivities are extremely small compared to the quantity $\dot{\gamma} a^2$ representing the mean motion,
3. anisotropy and non-coaxiality are negligible compared to mean diffusivity, even for simple shear (**G**),
4. diffusivities for the planar deformations (**P** and **G**) are comparable and an order of magnitude smaller than for the three-dimensional deformations (**U** and **B**), and
5. all diffusivities appear to be strongly dependent on packing density.

Hence, we conclude that fluctuations and the associated diffusivity are nearly isotropic, with strong dependence on magnitude of the third invariant of the shearing $\mathbf{E}^{\diamond}$ and on packing density ρ, and with much weaker dependence on vorticity or plastic 'spin', representing material rotation of the principal axes of **S**. Neither rotational diffusivities derived from $\mathbf{w}'$ nor contributions to diffusivity of the type $\mathbf{I}_{AB}$ are reported here, since these were found to be an order of magnitude smaller that the companion diffusivities displayed in Figs 2 and 3. The smallness of $\mathbf{I}_{AB}$ indicates surprisingly weak pair correlations and suggests that the stochastic motion of arbitrary particle clusters should follow from single-particle statistics. This rather unexpected result may be limited to the relatively small plastic strains investigated here, whereas more important translational and rotational fluctuations could occur at the larger strains and smaller densities typical of the non-dilatant 'critical state' of soil mechanics (**19**). Next, we briefly explore some of the implications for 'fabric' evolution arising from the neglect of particle diffusion. In particular, we consider some plausible approximate forms for the distribution of unit contact normals **e** in a monodisperse sphere assembly, in the absence of a complete statistical mechanics for the assembly.

3.2 *Implications for fabric evolution and continuum plasticity models*

Given an appropriate evolution equation for the (radial) distribution $P_{\mathbf{r}}(\mathbf{r}, t)$ of separations $\mathbf{r} := r\mathbf{e}$ between particle pairs, one could in principle obtain an exact evolution equation for the distribution

[‡] Generally, (19) provides an acceptable definition of anisotropy whereas a more suitable measure is provided by the invariant $|\mathbf{SD} - \mathbf{DS}|/|\mathbf{D}||\mathbf{S}|$.

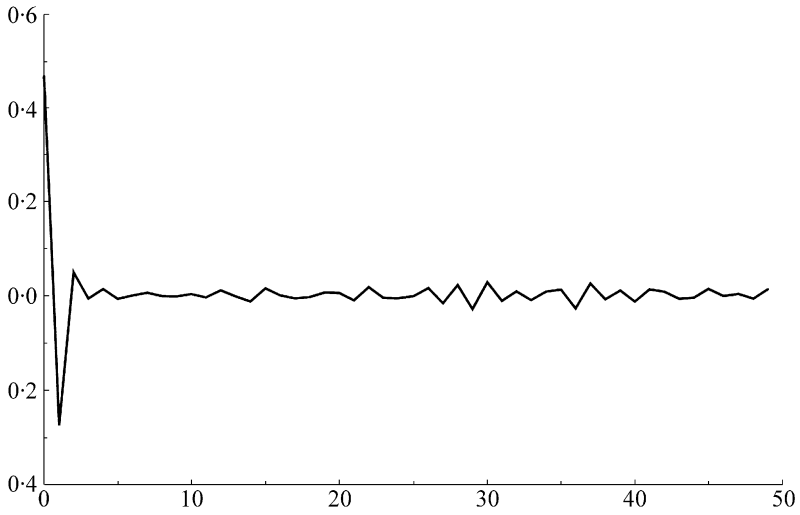

Fig. 1 A typical velocity component autocorrelation C *vs*. number of strain steps $\hat{\tau}$ (of magnitude $\Delta\gamma = 0{\cdot}0002$)

of unit contact normals $\mathbf{e}$ in a homogeneously deforming assembly. In particular, a flux of the general form

$$Q = \mathbf{e} \cdot (\overline{\mathbf{u}} P_{\mathbf{r}} - \mathbf{D} \nabla_{\mathbf{r}} P_{\mathbf{r}})_{r=2} \tag{20}$$

onto the contact surface $r = 2$ would give the rate of creation (or loss) of contacts in the balance

$$\frac{\partial P}{\partial t} + \nabla_{\mathbf{e}} \cdot \overline{\omega} P = Q \tag{21}$$

for the distribution $P(\mathbf{e}, t)$ of contacts on the unit sphere Ω. We note that a similar equation for two-dimensional assemblies has been proposed in (**20**). Here, $\overline{\omega} \equiv \dot{\mathbf{e}} = \Lambda \mathbf{e}$, with $\Lambda = (\mathbf{1} - \mathbf{e} \otimes \mathbf{e})\mathbf{L}$, is advection on Ω, given by the orthogonal projection of the velocity gradient (1) onto Ω at $\mathbf{e}$ (**21**), and we have neglected diffusion on Ω in (21). If the radial diffusion, represented by $\mathbf{D}$ in (20), is also negligible, we have

$$Q = -k P(\mathbf{e}, t), \quad \text{where } k := -u_r(\mathbf{r}, t) P_{\mathbf{r}}(\mathbf{r}, t)(\mathbf{r}, t)|_{r=2} / P(\mathbf{e}, t). \tag{22}$$

In the special case of a time-independent radial velocity $u_r(\mathbf{r}, t) = u_r(\mathbf{r})$ and a probability distribution $P_{\mathbf{r}}(\mathbf{r}, t) = P_r(\mathbf{r}) P(\mathbf{e}, t)$, the quantity k in (22) is given by $k = k(\mathbf{e})$, a function depending on the limiting radial velocity and probability distributions and representing collisional contact generation ($k < 0$) or loss ($k > 0$). In the absence of a complete statistical mechanics, we resort to an approximate form of (21), with k treated as a known function $k = k(\mathbf{e}, \mathbf{L})$, a function which may also be construed to depend in a self-consistent way on various averages or 'fabric tensors' derived from appropriate solutions to (21). This approximation, which resembles the well-known Krook kinetic approximation to the Boltzmann equation of kinetic theory (**22**), represents

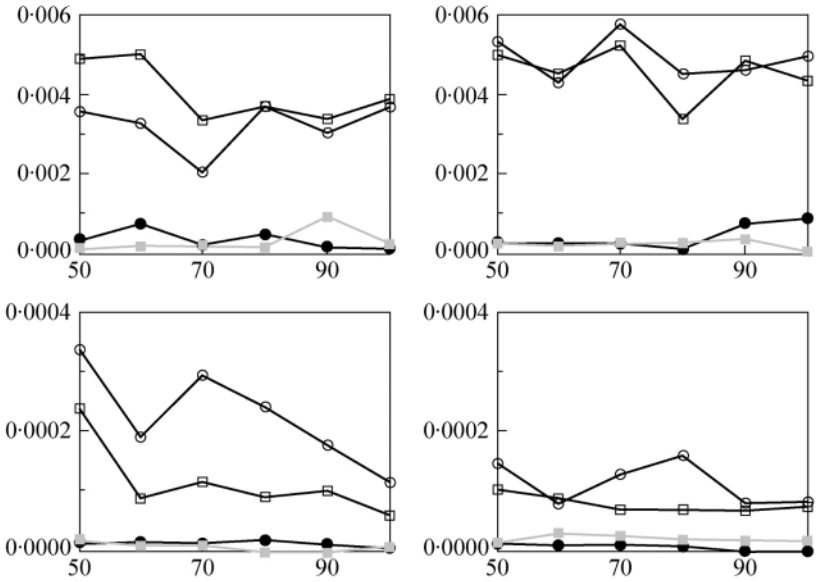

Fig. 2 Various self diffusivities D_{AA} *vs.* total number of strain steps $\hat{T}$, for density $\rho = 0{\cdot}63$. Left-hand subplots correspond to friction coefficient $\mu = 0{\cdot}5$, right-hand to $\mu = 0{\cdot}1$. In the upper subplots empty circles and squares lying near 0·005 refer, respectively, to mean uniaxial and biaxial self-diffusivities D_0. Filled circles and squares refer to 'non-coaxiality' D_2 in the two diffusivities. A similar convention is employed in the lower subplots, with uniaxial and biaxial diffusivities replaced by those for pure shear and simple shear, respectively

a somewhat less general form than that proposed in (**20**) for the special case of two-dimensional granular assemblies. With this restricted form of (22), the balance (21) is then separable according to $P(\mathbf{e}, t) = f(\mathbf{e}, t)n(\mathbf{e}, t)$, where f and n satisfy separate balances,

$$\dot{n} = -kn \quad \text{and} \quad \dot{f} = -(\nabla_e \cdot \overline{\omega})f, \tag{23}$$

where

$$\dot{(\ )} = \frac{\partial(\ )}{\partial t} + \overline{\omega} \cdot \nabla(\ ).$$

Now, the material derivative $\dot{(\ )}$ represents a partial derivative at constant $\mathbf{e}_0$ associated with the reciprocal mappings

$$\mathbf{e}(\mathbf{e}_0, t) = \frac{\mathbf{F}\mathbf{e}_0}{|\mathbf{F}\mathbf{e}_0|} \qquad \text{and} \qquad \mathbf{e}_0(\mathbf{e}, t) = \frac{\mathbf{F}^{-1}\mathbf{e}}{|\mathbf{F}^{-1}\mathbf{e}|}, \tag{24}$$

where the deformation gradient $\mathbf{F}$ satisfies standard equations, $\dot{\mathbf{F}} = \mathbf{L}\mathbf{F}$, with $\mathbf{F}(0) = \mathbf{1}$,

$$\det \mathbf{F} = \frac{\rho_0}{\rho} = \exp\left\{\int_0^t \dot{\epsilon}_V \, dt\right\} \tag{25}$$

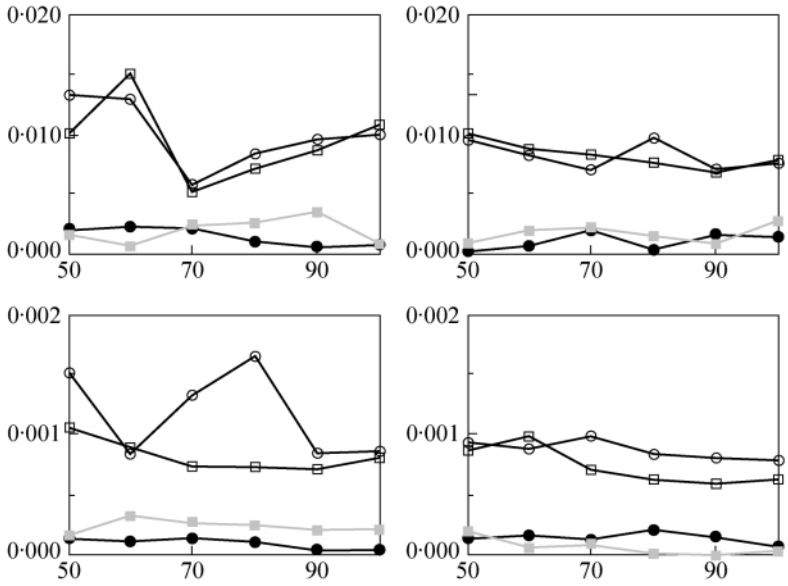

Fig. 3 Same as Fig. 2, except that $\rho = 0{\cdot}56$

and $\dot{\epsilon}_V = \mathrm{tr}\{\mathbf{L}\} = \nabla \cdot \overline{\mathbf{u}}$. Here, as below, subscripts 0 refer to initial state $t = 0$. We note that the density ratio ρ_0/ρ is determined by (25) and dilatancy through

$$\int_0^t \dot{\epsilon}_V \, dt \equiv \int_0^\gamma \frac{d\epsilon_V}{d\gamma} \, d\gamma.$$

After some calculus, the solutions to (23) can be written down explicitly as

$$f(\mathbf{e}, t) = f_0\{\mathbf{e}_0(\mathbf{e}, t)\}J \quad \text{and} \quad n(\mathbf{e}, t) = n_0\{\mathbf{e}_0(\mathbf{e}, t)\} \exp\left\{-\int_0^t K(t') \, dt'\right\},$$

where $J \equiv d\Omega_0/d\Omega = (\det \mathbf{F})/|\mathbf{F}\mathbf{e}_0|^3$ is the Jacobian for (24),

$$K(t') = k\{\mathbf{e}_t(t'), \mathbf{L}(t')\} \quad \text{and} \quad \mathbf{e}_t(t') = \frac{\mathbf{F}_t(t')\mathbf{e}}{|\mathbf{F}_t(t')\mathbf{e}|}$$

with $\mathbf{F}_t(t') = \mathbf{F}(t')\mathbf{F}^{-1}(t)$ being standard notation for relative deformation gradient. We note that in the case where breakage k is independent of $\mathbf{e}$ then n reduces to global contact density (number of contacts in unit volume of assembly), $n(t) = \int_\Omega P \, d\Omega$, and $f(\mathbf{e}, t)$ is then simply the fraction lying in solid angle $d\Omega(\mathbf{e})$. The preceding relations, which bear a strong resemblance to those obtained for the director orientation in theories of liquid crystals (cf. (**21**)), obviously allow one to compute various fabric tensors $\langle \mathbf{e} \otimes \mathbf{e} \rangle$, $\langle \mathbf{e} \otimes \mathbf{e} \otimes \mathbf{e} \otimes \mathbf{e} \rangle$, ... It is evident from the above that further progress depends on knowledge of how dilatancy $d\epsilon_V/d\gamma$ and contact breakage k depend on kinematics and microstructure. Within the limits of the approximate model put forth above, one can thus

envisage a theoretical program in which plausible forms for both dilatancy and contact breakage, specified either by experiment, simple theory or numerical simulation, would allow for prediction of the evolution of contact-normal distribution in idealized assemblies. To illustrate the simplest phenomenological model, suppose that k is given as an expansion for small fabric anisotropy by

$$k = \alpha\dot{\epsilon}_V + \beta \mathrm{tr}\{\mathbf{A}^{\diamond}\mathbf{S}^{\diamond}\} + O(\mathbf{A}^{\diamond 2}), \tag{26}$$

where α and β are constants independent of $\mathbf{e}$, and $\mathbf{A}$ denotes the well-known fabric tensor

$$\mathbf{A} = \langle \mathbf{e} \otimes \mathbf{e} \rangle_f = \mathbf{F}\left\{ \int_{\Omega} f_0(\mathbf{e}_0) \left(\frac{\mathbf{e}_0 \otimes \mathbf{e}_0}{\mathbf{e}_0 \cdot \mathbf{C}\mathbf{e}_0} \right) d\Omega(\mathbf{e}_0) \right\} \mathbf{F}^T \tag{27}$$

with $\mathbf{C} = \mathbf{F}^T\mathbf{F}$ denoting a standard strain measure. Retention of only the first term in (26) gives the immediate relation between contact density and overall density,

$$n/n_0 = (\rho/\rho_0)^{\alpha}, \tag{28}$$

while inclusion of the second term in (26) leads to a correction for anisotropy. We note that (27) and (28) represent special cases of more general structural-evolution equations,

$$\overset{\circ}{\mathbf{A}} = \mathbf{g}(n, \mathbf{A}; \mathbf{S}) \quad \text{and} \quad \dot{n} = h(n, \mathbf{A}; \mathbf{S}), \tag{29}$$

where $\mathbf{g}$ and h are homogeneous degree-one in strain rate $\mathbf{S}$. For a complete description of granular plasticity, one further needs a a fabric-dependent model for stress $\mathbf{T}$, that is, a yield surface of the general form proposed by (**23**)

$$\mathcal{F}(n, \mathbf{A}, \mathbf{T}; \mathbf{S}) = 0. \tag{30}$$

Of course, cubical-triaxial tests and simulations of the type presented here cannot determine the general analytical form for (27) to (30), a matter which requires more detailed micromechanical analysis or phenomenological modelling. With no attempt at a comprehensive review, we cite here a few examples. In the stress-dilatancy theory of Rowe (**1**), the subject of several critical reviews (**24**, **25**), (30) is homogeneous degree-zero in $\mathbf{T}$ and the dependence on $\mathbf{S}$ reduces to a simple dependence on dilatancy $d\epsilon_V/d\gamma$. The first property is to be expected of assemblies of non-cohesive rigid granules having no intrinsic stress scale, such as those in the present simulations. The second property is special to Rowe's theory and gives stress ratios in terms of dilatancy, presumably through a relation like the right-hand equation in (27). However, Rowe's theory is mainly restricted to cubical-triaxial tests, representing some better than others, and it does not capture complex path dependence represented generally by (27) to (30), (**1**, **25**). While the recent mean-field theory of (**4**) provides a general analytical form of the type (30), it does not offer a description of large-scale fabric evolution of the form (27). In the realm of phenomenological plasticity, including various classical incremental models, evolution is described by means of equations of the so-called 'hypoelastic' (**8**) or 'hypoplastic' variety (cf. (**26**)), which may be thought of as arising from restricted forms of (30). For example, in the absence of dependence on $\mathbf{A}$, (28) and (30) represent a form of 'critical-state' soil mechanics (**19**). More general hypoplastic models arise as generalizations of De Josselin De Jong's 'double-sliding' model (**27**), which has been reviewed and extended by others, notably

(**28** to **30**)[§]. Such models might arise from (27), together with a special form of (30) connecting **T** and **A**, independently of n and **S**. Whenever **A** can be eliminated, (27) gives a hypoplastic evolution equation for **T**, without explicit reference to the original yield surface (**26**). However, as recognized by (**30**), such restricted models do not allow for the evolution of fabric and dilatancy beyond some isotropic 'initial' state. It is therefore clear that a more complete statistical mechanics is called for. While various mean-field models of the type discussed above might be hoped appropriate to this task, the following consideration might suggest otherwise.

4. Possible effects of fluctuations

One possible test of the MFA is the prediction of Reynolds dilatancy, which we recall gives the yield stress for frictionless particles (**7**). In the work just cited, an effort was made to improve systematically on the purely kinematic estimate of Reynolds (**31**) for the dilatancy of random close-packed sphere assemblies, an estimate which appears to involve a mean-field approximation. We recall that the Reynolds estimate can be written in the present notation as

$$\frac{1}{\sqrt{3}}\frac{d\epsilon_V}{d\gamma} \equiv \tan \nu_D = 2^{-\frac{3}{2}} \cos\phi, \tag{31}$$

where ν_D is the dilatancy angle of (**7**) and ϕ the Lode angle of Table 1 and (12). In one interpretation, denoted by 'Reynolds A' in (**7**), one takes $\tan \nu_D \equiv 2^{-\frac{3}{2}} = 0{\cdot}35355\ldots$, strictly appropriate to uniaxial compression $\phi = 0$, as applicable to arbitrary deformations, whereas in another interpretation, 'Reynolds B', one employs the more general relation (31). These two interpretations lead to cones with cross-sections sketched as the two innermost curves in the polar plot (in 10-degree increments) of $\tan \nu_D$ *vs.* Lode angle ϕ in Fig. 8 (p. 428). We recall that these curves also represent yield surfaces for frictionless particles ($\mu = 0$) (**7**). A potentially more accurate estimate was offered in (**7**), based on the dilation of a set of statistically representative, space-filling volume elements subject to the global shearing $\mathbf{E}^{\diamond}$. In particular, the representative element or 'simplex' is taken to be a Delaunay tetrahedron, having (four) vertices that represent nearest neighbours and (six) edges or 'bonds' which are classified as 'active' or 'inactive', depending on whether neighbours are in contact or not. A given simplex, generated by a Monte-Carlo sampling of Euler angles, is allowed to dilate just enough to offset the shear-induced compression of its maximally compressed active bond, and the average dilation is then calculated for the assembly. In the absence of sufficiently accurate packing statistics, the representative simplex for a dense random packing was assumed in (**7**) to be a regular, fully-connected and randomly oriented tetrahedron, with six active bonds. This results in the outermost curves in Fig. 8, corresponding to tetrahedra of the body-centred cubic (bcc) packing and hexagonal-close or face-centred cubic packing (hcp) forms, respectively. The increased number of particles in the present work (500 *vs.* ≈ 50 per computation cell) provides greatly improved shape statistics for the Monte-Carlo simulation proposed in (**7**), which we now exploit.

[§] According to (**30**), the dilatant double-sliding model can be written in the present notation as $[\mathbf{T}, \overset{\circ}{\mathbf{T}}] = \sigma[\mathbf{S}, \mathbf{T}]$, where $[\mathbf{A}, \mathbf{B}] := \mathbf{AB} - \mathbf{BA}$ denotes the commutator (Lie product), and σ is a scalar variable involving dilatancy and friction angle. At least one solution of this equation is given by the hypoplastic form $\overset{\circ}{\mathbf{T}} = \sigma\mathbf{S} + |\mathbf{S}^{\diamond}| g(\mathbf{T})$, where g is an isotropic tensor function, that is, a second-degree polynomial, $g(\mathbf{T}) = a\mathbf{1} + b\mathbf{T} + c\mathbf{T}^2$, with scalar coefficients a, b, c depending on the principal invariants of **T**.

4.1 *Simplex statistics*

From the many possible ways to parametrize simplex statistics, we choose to employ the deformation gradient $\mathbf{F} \equiv \mathbf{F}_{\mathcal{S}}$ representing the homogeneous linear transformation which carries a given Delaunay tetrahedron $\mathcal{S}$ from a reference state to its current state. Note that the (nine) components of $\mathbf{F}$ plus the (three) coordinates defining the position of any vertex serve to represent the relevant configuration vector $\mathbf{q}$ in (6) and the (twelve) translational degrees of of freedom of the particles defining tetrahedral vertices. Note also that in any actual deformation of a particle assembly $\mathbf{F}$ represents a non-singular transformation, except for deformations that give rise to topological rearrangement involving exchange of nearest neighbours. We may then represent *shape* and *orientation* of a simplex, required for the dilatancy estimate of Goddard and Didwania (**7**), by means of the standard *polar decomposition*: $\mathbf{F} = \mathbf{RV}$, where $\mathbf{R}$ is a proper orthogonal tensor representing the *finite rotation* and $\mathbf{V}$ is the symmetric positive-definite (*right*) *stretch*[¶] representing strain. We can then define the configuration of a Delaunay tetrahedron by means of the deformation from a standard shape, in particular an equilateral tetrahedron with edge-length 2 (one sphere diameter) and with given orientation relative to fixed axes. Thus, the transformation of any three edges from the reference configuration to the actual configuration yields the necessary (nine) linear equations for $\mathbf{F}$ for every simplex in the assembly, and the spectral technique discussed in (**32**) permits rapid computation of the associated rotation $\mathbf{R}$ and strain $\mathbf{V}$. For random isotropic packings, the dilatancy estimate of (**7**) requires only the statistics of $\mathbf{R}$, represented, for example, by three Euler angles $\alpha \in [0, 2\pi]$, $\beta \in [0, \pi]$, $\gamma \in [0, 2\pi]$, plus the probability of active contacts between nearest neighbours. In the Monte-Carlo implementation of Goddard and Didwania (**7**), the quantities

$$\tfrac{1}{2}(\alpha/\pi), \quad \tfrac{1}{2}(1 + \cos\beta) \quad \text{and} \quad \tfrac{1}{2}(\gamma/\pi)$$

are chosen from a uniform distribution on [0, 1] and the probability of active contact is taken to be identically equal to unity, whereas in the present work we employ the same Monte-Carlo technique but make use of the actual packing statistics obtained from the initial sphere packing. Hence, the Euler-angle and contact probabilities are chosen from distributions obtained by the smoothing of histograms like those shown in Figs 4 to 7. While Figs 4 to 6 confirm the above distribution of Euler angles assumed in (**7**), Fig. 7 implies a far smaller probability of active contacts, which appears to account for most of the reduction in the present estimate of dilatancy, shown as one of the intermediate curves in Fig. 8. One notes also that the present dilatancy estimate may still represent an upper bound for the case of frictionless spheres ($\mu = 0$), as conjectured in (**7**). It can also be seen that all the mean-field estimates, including (31), that of (**7**) and the improvement just proposed, yield similar trefoil-shaped curves in Fig. 8, and that this shape is quite different from the curve given by the full mechanics simulation. To us, the most plausible explanation for this failure of the MFA is fluctuations near mechanically unstable equilibrium points, such as those associated with the uniaxial compression $\mathbf{U}$. Near such points, any pair of neighbouring particles whose line of centres happens to lie close to the major axis of compression will have a tendency to rotate, much more rapidly than indicated by the mean deformation, to stable positions with a much smaller contribution to volume expansion. Such a mechanism could account for the more rapid 'roll off' of dilatancy *vs.* Lode angle near $\phi = 0$ exhibited by the mechanics simulations in Fig. 8. This same effect may account for similar changes of shape of the yield surfaces shown as (**7**, Figs 3 and 4), as

[¶] In the standard continuum mechanics literature (**8**) this is denoted by $\mathbf{U}$, the symbol reserved here for the uniaxial compression listed in Table 1.

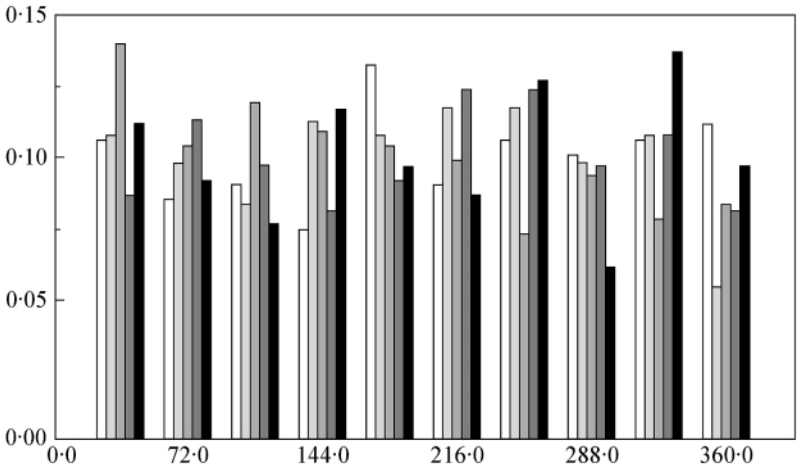

Fig. 4 Relative frequencies of the (Euler) orientation angles for Delaunay tetrahedra in a random isotropic assemblies of 500 equal spheres with $\rho = 0{\cdot}63$: Frequency of α *vs.* α (degrees). Different shaded bars represent each of five random packings

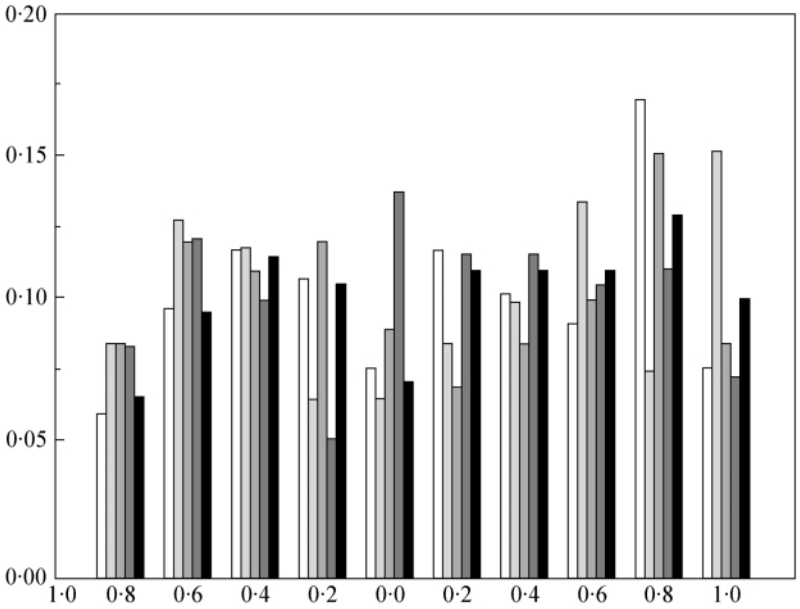

Fig. 5 Relative frequencies of the (Euler) orientation angles for Delaunay tetrahedra in a random isotropic assemblies of 500 equal spheres with $\rho = 0{\cdot}63$. Frequency of $\cos\beta$ *vs.* $\cos\beta$. Different shaded bars represent each of five random packings

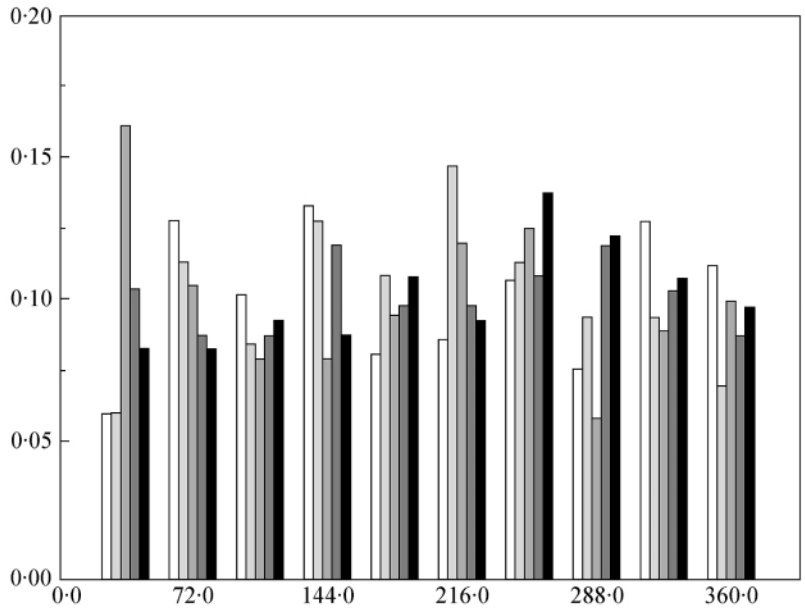

Fig. 6 Relative frequencies of the (Euler) orientation angles for Delaunay tetrahedra in a random isotropic assemblies of 500 equal spheres with $\rho = 0{\cdot}63$. Frequency of γ *vs.* γ (degrees). Different shaded bars represent each of five random packings

well as the magnitudes of uniaxial ('triaxial') stresses. There is an interesting question as to whether such effects might be captured by an appropriate asymptotic analysis for weak fluctuations in (5) or small diffusivity in (6), such as those employed in other diffusion–convection problems with large Péclet number.

5. Conclusions

The main conclusions are summarized above in the abstract. While the postulated statistical mechanics is rendered more plausible by our finding of small fluctuations, we believe that results from our quasi-static algorithm should be compared against dynamic simulations, of the 'molecular-dynamics' variety, to investigate *inter alia* the possible effects of micro-inertia. If further validated by such calculations, the postulated model appears to offer a convenient theoretical framework for describing the effective continuum properties of granular assemblies. The interesting problem remains of estimating the effect of small but non-zero diffusivity on various mechanical properties.

Acknowledgements

Partial support from the US National Aeronautics and Space Administration (grant NAG3-1888), the US Air Force Office of Scientific Research (grant F49620-96-1-0246), and the National Science Foundation (grant CTS-9510121) is gratefully acknowledged. The second author also acknowledges a Koranyi Scholarship from the Cholnoky Foundation.

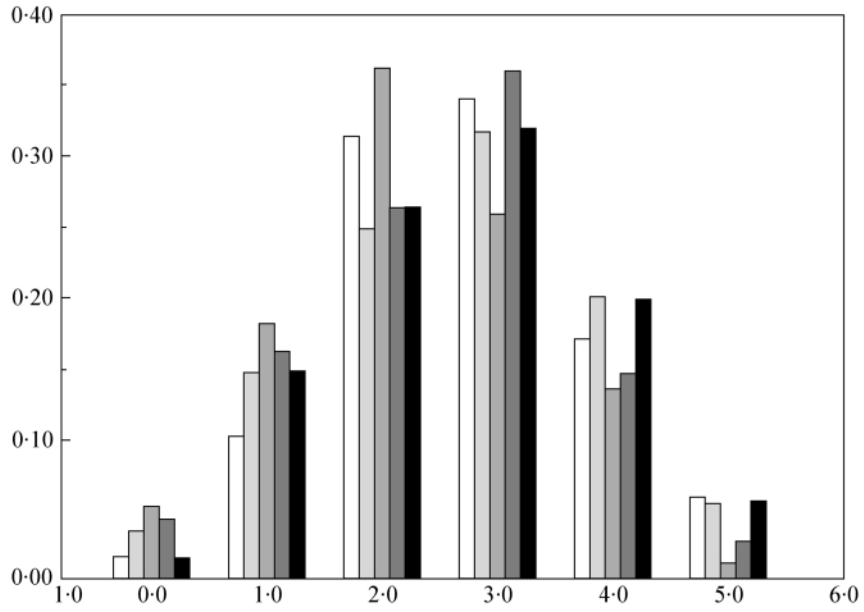

Fig. 7 Relative frequency of number of contacts per particle (coordination number) for the assemblies of Figs 4 to 6

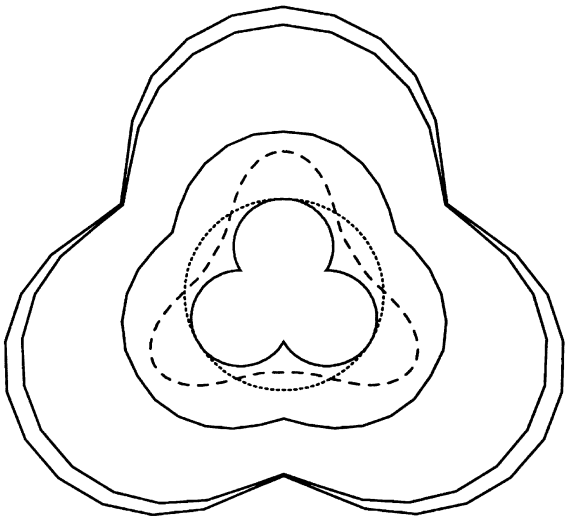

Fig. 8 Cross-sections of various dilatancy cones. Two innermost curves: 'Reynolds A' (outer dotted line) and 'Reynolds B' estimates (**7**). Two outermost curves: Simplified mean-field estimate of (**7**) for hcp (outer) and bcc packings. Two intermediate curves: complete mechanics simulation (dashed line), for initially random monodisperse assembly of Figs 4 to 6 with $\mu = 0$, subject to plastic strain $\gamma = 0{\cdot}001$, and improved mean-field estimate (solid line) based on actual statistics of Euler angles and contacts represented in Figs 4 to 7

References

1. P. W. Rowe, *Proc. R. Soc.* A **269** (1962) 229–236.
2. K. Walton, *J. Mech. Phys. Solids* **35** (1987) 213–226.
3. A. Jagota and C. Y. Hui, *J. Appl. Mech.* **57** (1990) 789–791.
4. J. T. Jenkins and O. D. L. Strack, *Mech. Mater.* **16** (1993) 25–33.
5. X. Zhuang, A. K. Didwania and J. D. Goddard, *J. Comput. Phys.* **121** (1995) 331–346.
6. J. D. Goddard, In *Physics of Dry Granular Media (Proc. NATO ASI, Cargèse 1997)* (ed. H. Herrmann, J.-P. Hovi and S. Luding; Kluwer Academic, Dordrecht 1998) 1–24.
7. —— and A. K. Didwania, *Q. Jl Mech. Appl. Math.* **51** (1998) 15–43.
8. C. Truesdell and W. Noll, The non-linear field theories of mechanics, *Handbuch der Physik*, Vol. III/3 (ed. S. Flügge; Springer, Berlin 1965).
9. J. F. Brady and G. Bossis, Stokesian dynamics, *Ann. Rev. Fluid Mech.* **20** (1988) 111–157.
10. I. Karatzas and S. E. Shreve, *Brownian Motion and Stochastic Calculus* (Springer, Berlin 1988).
11. N. G. Van Kampen, *Stochastic Processes in Physics and Chemistry* (North–Holland, Amsterdam 1992).
12. D. Leighton and A. Acrivos, *J. Fluid Mech.* **181** (1987) 415–439.
13. J. T. Jenkins and D. F. McTigue, In *Two Phase Flows and Waves* (ed. D. D. Joseph and D. G. Schaeffer; Springer, Berlin 1990) 70–79.
14. P. R. Nott and J. F. Brady, *J. Fluid Mech.* **275** (1994) 157–199.
15. I. Frankel and H. Brenner, *ibid.* **230** (1991) 147–181.
16. M. P. Allen and D. J. Tildesley, *Computer Simulation of Liquids* (University Press, Oxford 1987).
17. S. Fortune, In *Euclidean Geometry and Computers* (ed. D. A. Du and F. K. Hwang; World Scientific, River Edge 1992) 193–233.
18. D. A. McQuarrie, *Statistical Mechanics* (Harper & Rowe, New York 1976).
19. A. Schofield and P. Wroth, *Critical State Soil Mechanics* (McGraw–Hill, New York 1968).
20. S. Roux and F. Radjai, In *Physics of Dry Granular Media (Proc. NATO ASI, Cargèse 1998)* (ed. H. Herrmann, J.-P. Hovi and S. Luding; Kluwer Academic, Dordrecht 1997) 229–236.
21. M. Doi, *J. Polym. Sci.* **19** (1981) 229–243.
22. J. H. Ferziger and H. G. Kaper, *Mathematical Theory of Transport Processes in Gases* (North–Holland, Amsterdam 1972).
23. S. C. Cowin, *Mech. Mater.* **5** (1986) 251–260.
24. P. W. Rowe, In *Proc. Roscoe Memorial Symposium 'Stress–Strain Behaviour of Soils'* (ed. R. H. G. Parry; G. T. Foulis, London 1972) 143–194.
25. J. Feda, *Mechanics of Particulate Media—The Principles* (Elsevier, Amsterdam 1982).
26. W. Wu, E. Bauer and D. Kolymbas, *Mech. Mater.* **23** (1996) 45–69.
27. G. De Josselin De Jong, *Géotechnique* **21** (1971) 155–163.
28. A. J. M. Spencer, *J. Mech. Phys. Solids* **12** (1964) 337–351.
29. R. Butterfield and R. M. Harkness, The kinematics of Mohr–Coulomb materials, *Proc. Roscoe Memorial Symposium, 'Stress–Strain Behaviour of Soils'* (ed. R. H. G. Parry; G. T. Foulis, London 1972) 220–233.
30. M. M. Mehrabadi and S. C. Cowin, *J. Mech. Phys. Solids* **26** (1978) 269–284.
31. O. Reynolds, *Phil. Mag.* **20** (1885) 469–481.
32. J. D. Goddard and K. Ledniczky, *J. Elast.* **47** (1997) 255–259.